The *Shigella flexneri* effector IpaH1.4 facilitates RNF213 degradation and protects cytosolic bacteria against interferon-induced ubiquitylation

Running title:

***Shigella* IpaH1.4 inhibits host ubiquitin ligase RNF213**

Luz Saavedra-Sanchez[a], Mary S. Dickinson[a], Shruti Apte[a], Yifeng Zhang[a], Maarten de Jong[b], Samantha Skavicus[a], Nicholas S. Heaton[a], Neal M. Alto[b], and Jörn Coers[a,c,#]

[a]Department of Molecular Genetics and Microbiology, Duke University Medical Center, Durham, NC 27710, USA

[b]Department of Microbiology, University of Texas Southwestern Medical Center, Dallas, TX 75390, USA.

[c]Department of Integrative Immunobiology, Duke University Medical Center, Durham, North Carolina, USA

#Correspondent footnote: Department of Molecular Genetics and Microbiology, Duke University Medical Center, Durham, NC 27710, USA. Email: jorn.coers@duke.edu

ABSTRACT

A central signal that marshals host defense against many infections is the lymphocyte-derived cytokine interferon-gamma (IFNγ). The IFNγ receptor is expressed on most human cells and its activation leads to the expression of antimicrobial proteins that execute diverse cell-autonomous immune programs. One such immune program consists of the sequential detection, ubiquitylation, and destruction of intracellular pathogens. Recently, the IFNγ-inducible ubiquitin E3 ligase RNF213 was identified as a pivotal mediator of such a defense axis. RNF213 provides host protection against viral, bacterial, and protozoan pathogens. To establish infections, potentially susceptible intracellular pathogens must have evolved mechanisms that subdue RNF213-controlled cell-autonomous immunity. In support of this hypothesis, we demonstrate here that a causative agent of bacillary dysentery, *Shigella flexneri,* uses the type III secretion system (T3SS) effector IpaH1.4 to induce the degradation of RNF213. *S. flexneri* mutants lacking IpaH1.4 expression are bound and ubiquitylated by RNF213 in the cytosol of IFNγ-primed host cells. Linear (M1-) and lysine-linked ubiquitin is conjugated to bacteria by RNF213 independent of the linear ubiquitin chain assembly complex (LUBAC). We find that ubiquitylation of *S. flexneri* is insufficient to kill intracellular bacteria, suggesting that *S. flexneri* employs additional virulence factors to escape from host defenses that operate downstream from RNF213-driven ubiquitylation. In brief, this study identified the bacterial IpaH1.4 protein as a direct inhibitor of mammalian RNF213 and highlights evasion of RNF213-driven immunity as a characteristic of the human-tropic pathogen *Shigella.*

INTRODUCTION

The lymphocyte-derived cytokine IFNγ is a strong inducer of cell-autonomous immunity (1). The IFNγ-inducible E3 ubiquitin ligase ring finger protein 213 (RNF213) provides protection against a diverse group of intracellular pathogens that includes viruses, protozoa, and bacteria (2-8). RNF213 binds to bacteria that enter the host cell cytosol. Once bound to Gram-negative bacteria such as *Salmonella*, RNF213 directly ubiquitylates the bacterial surface molecule, lipopolysaccharide (LPS). These ubiquitylated cytosolic bacteria can be captured by ubiquitin-binding proteins and delivered into autolysosomes for degradation (3).

While the predominantly vacuolar pathogen *Salmonella* is susceptible to RNF213-mediated cytosolic host defense (3), the cytosol-adapted Gram-negative pathogen *Burkholderia thailandensis* is resistant. *B. thailandensis* escapes RNF213-driven host defense in part through the secretion of the virulence factor TssM, a ubiquitin esterase that removes ubiquitin from LPS on the bacterial surface (9). However, whether and how other cytosolic bacterial pathogens escape from RNF213-driven ubiquitylation is unknown.

Shigella spp. are the etiological agent of bacillary dysentery and a leading cause of diarrheal deaths, malnutrition, and growth retardation in children (10-12). *Shigella* spp. invade the intestinal epithelium, enter the host cell cytosol of infected human colonic epithelial cells, and trigger an acute inflammatory response that involves the secretion of IFNγ by lymphocytes (13-16). IFNγ signaling in epithelial cells induces the expression of human guanylate binding protein 1 (GBP1), a defense protein that blocks bacterial intracellular motility and cell-to-cell spread (17-20). To counter this potent cell-autonomous immune program, *Shigella flexneri* employs its type III secretion system (T3SS) to deliver the GBP1 inhibitor IpaH9.8 into the host cell cytosol. Loss of IpaH9.8 results in diminished *S. flexneri* virulence and a potent antibacterial host response (19-22).

IpaH9.8 belongs to a family of T3SS effectors that contain a leucine-rich repeat (LRR) domain involved in substrate recognition and a novel E3 ligase (NEL) domain that transfers K48-linked ubiquitin to its bound substrate (23). K48-linked ubiquitylation tags the substrate for proteasomal degradation. These IpaH proteins belong to a ‘second

wave' of T3SS effectors that are under the control of the transcriptional regulator MxiE. Second wave T3SS effectors have been shown to promote host cell survival, to dampen inflammation, and to counteract cell-autonomous immune programs (24), yet their full repertoire of targets remains to be determined.

In the present work we found that the MxiE-regulated T3SS effector IpaH1.4 facilities the proteasomal degradation of RNF213. Remarkably, RNF213 functions independent of the linear ubiquitin chain assembly complex (LUBAC) to promote the linear and lysine-linked ubiquitylation of *ipaH1.4*-deficient *S. flexneri* mutants. We observed that ubiquitylated *S. flexneri* continued to replicate inside the host cell cytosol, indicating that *S. flexneri* employs additional unknown virulence mechanisms to interfere with its degradation. Thus, our study demonstrates that the human enteric pathogen *S. flexneri* directly interferes with RNF213 expression and also limits host defense downstream of RNF213-driven ubiquitylation.

RESULTS

Deletion of *mxiE* renders *S. flexneri* susceptible to linear ubiquitylation

Previous studies identified a cell-autonomous host defense program in which mammalian cells attach linear ubiquitin (M1) to the surface of the Gram-negative pathogen *Salmonella enterica* upon bacterial spillage into the host cell cytosol (3, 25). Recently, it was reported that the cytosol-adapted pathogen *B. thailandensis* secretes a ubiquitin esterase that renders the bacteria resistant to this type of cytosolic ubiquitylation (9). We therefore hypothesized that resistance to host-driven linear ubiquitylation is a common feature of bacterial pathogens that are adapted to a cytosolic milieu. To test this concept, we monitored ubiquitylation of the professional cytosolic pathogen *Shigella flexneri* (serotype 2a, strain 257T) by immunofluorescence. We found that wildtype (WT) *S. flexneri* remained largely devoid of M1-linked ubiquitin in both alveolar A549 and colonic HT29 epithelial cell lines under both unprimed and IFNγ-primed conditions (Fig. 1A – C). In contrast to WT *S. flexneri,* a Δ*mxiE* mutant strain that has diminished expression of 'second-wave' T3SS effector proteins (26, 27), was robustly stained with anti-M1 antibodies in IFNγ-primed host cells (Fig. 1A – C). These observations indicate that *S. flexneri* uses MxiE-dependent effectors to evade an IFNγ-activated ubiquitylation pathway that targets cytosolic bacteria.

Linear and lysine-linked ubiquitin is attached to *S. flexneri* Δ*mxiE*

The ubiquitin protein contains seven lysine residues. Any of these lysine residues or the N-terminal methionine can form isopeptide bonds with the C-terminal glycine residue of ubiquitin to form chains. To determine which ubiquitin linkage types are present on the surface of *S. flexneri* Δ*mxiE* bacteria, we generated A549 cells that overexpressed internally tagged ubiquitin (INT-Ub) variants, which contain only a single lysine residue or lack lysines altogether. The lysine-less (7KR) variant can only be assembled into ubiquitin chains via its N-terminal methionine. We found that 7KR INT-Ub robustly co-localized with *S. flexneri* Δ*mxiE,* albeit with diminished efficiency compared to WT INT-Ub (Fig.2A). These data confirmed that M1-linked ubiquitin is bound to *S. flexneri* Δ*mxiE* but also indicated that other additional ubiquitin linkage types are attached to *mxiE*-deficient

bacteria. The functional importance of these lysine-linked ubiquitin chains was demonstrated by improved bacterial targeting of INT-Ub variants that can form additional K27-linkages or both K27- and K63-linkages (Fig. 2A). Linkage-specific antibodies against K27 and K63 confirmed that these two linkage types are present on *ΔmxiE* bacteria in IFNγ-primed A549 cells (Fig. 2B-C). Staining with an antibody that detects most ubiquitin linkage types (FK2) showed near complete overlap with anti-M1 staining (Fig. 2D-E). Because the percentage of FK2-positve but M1-negatve bacteria (Fig. 2E). was much smaller than the percentage of bacteria that were K27- or K63-positive (Fig. 2B-C), these data suggest that most *S. flexneri ΔmxiE* bacteria are decorated with both linear and lysine-linked ubiquitin.

The ubiquitylation of *S.flexneri ΔmxiE* is dependent on RNF213 but not LUBAC

Previous work showed that the multimeric E3 ligase LUBAC can deposit M1-linked ubiquitin on the surface of cytosolic *S. enterica* Typhimurium (25). Moreover, *S. flexneri* secretes the MxiE-regulated effector IpaH1.4 which specifically recognizes and marks the LUBAC components HOIP and HOIL-1 for proteasomal degradation (28-30). Consequently, we hypothesized that LUBAC was essential for the ubiquitylation of *ΔmxiE.* To test this hypothesis, we infected HOIP- and HOIL-1-deficient A549 cells ($HOIP^{KO}$, $HOIL\text{-}1^{KO}$, Fig. 3A) with the *ΔmxiE* mutant under IFNγ-primed conditions. Unexpectedly, deletion of either HOIP or HOIL-1, each an essential component of the LUBAC complex, did not diminish linear ubiquitylation of *ΔmxiE* when compared to WT cells (Fig.3B). Similarly, the internally tagged 7KR-Ub variant decorated *S. flexneri ΔmxiE* independent of the LUBAC component HOIP (Fig. 3C). Collectively, these data demonstrate that LUBAC is dispensable for linear ubiquitylation of *ΔmxiE* bacteria in the host cell cytosol of IFNγ-primed A549 cells.

The ubiquitin E3 ligase RNF213 was recently shown to ubiquitylate pathogen-containing vacuoles (2, 4) as well as Gram-positive and Gram-negative bacteria inside the host cell cytosol (3, 6, 9). Like HOIL-1, RNF213 is an IFNγ-inducible protein (Fig. 3A and (2, 4)). Using immunofluorescence microscopy, we detected RNF213 on the surface of *ΔmxiE* but not WT bacteria in IFNγ-primed A549 as well colonic HT29 cells (Fig. 3D-G). The vast majority of ubiquitylated *S.flexneri ΔmxiE* mutants (~93%) co-stained with

anti-RNF213 (Fig.3G), indicative of a functional role for RNF213 in the ubiquitylation of *ΔmxiE* bacteria. To directly probe for RNF213 function, we infected a pool of CRISPR-generated A549 RNF213^{KO} cells (Fig. 3A) with *S. flexneri ΔmxiE* and stained these IFNγ-primed cells for M1-, K27-, and K63-linked ubiquitin. We found that in the absence of human RNF213, antibodies specific for M1-, K27-, and K63-linked ubiquitin no longer stained the surface of *S.flexneri ΔmxiE* (Fig. 3B and 3H-I). In agreement with these immunofluorescence data, both WT and lysine-less ubiquitin (7KR-Ub) localized to *ΔmxiE* bacteria in WT but not in RNF213^{KO} cells (Fig. 3C). Together, these data demonstrate that human RNF213 is essential for the linear and lysine-linked ubiquitylation of MxiE-deficient *S. flexneri* mutants.

S. flexneri virulence factors IpaH1.4 and IpaH2.5 are sufficient to induce RNF213 degradation

The transcription factor MxiE induces the expression of several secreted effector proteins of the IpaH family that act as bacterial ubiquitin E3 ligases and tag host proteins for proteasomal degradation (20, 22, 28, 29, 31-35). Since our data revealed that the *S. flexneri* virulence factor MxiE blocks bacterial ubiquitylation by RNF213, we hypothesized that *S. flexneri* infections induce the proteasomal degradation of RNF213 in a MxiE-dependent manner. To test this hypothesis, we measured RNF213 protein levels by immunoblotting in cells that had been infected with WT or *ΔmxiE S. flexneri*. Our data revealed that RNF213 protein levels are drastically reduced upon infection with WT *S. flexneri* and that the deletion of *mxiE* partially restored RNF213 expression in infected cells (Fig.4A).

To directly test whether *S. flexneri* promote proteasomal degradation of RNF213, we conducted infections in the presence of the proteasomal inhibitor MG132. As expected, MG132 largely restored RNF213 total protein levels in *S. flexneri*-infected cells (Fig.4B). We next tested whether specific IpaH effector facilitates the degradation of RNF213. To this end, we transiently expressed GFP-fusion proteins of individual IpaH family members in HEK 293T cells that ectopically expressed RNF213 and measured their effects on RNF213 protein levels by immunoblotting. Our mini-screen revealed that the ectopic expression of the two closely related paralogs IpaH1.4 and IpaH2.5 were

sufficient to promote RNF213 degradation in HEK293T cells (Fig. 4C). Of note, substrate-binding LRR domains of IpaH2.5 and IpaH1.4 are 98.9% identical in DNA sequence and were previously shown to have comparable substrate specificity and functional redundancy (28). Both IpaH1.4 and 2.5 share a highly conserved NEL E3 ubiquitin ligase domain that contains an essential catalytic cysteine residue at position 368 (29). Catalytically inactive forms of IpaH1.4 or IpaH2.5, in which Cys368 is mutated to a serine (C/S), failed to degrade RNF213 (Fig. 4D). As an additional control we included overexpression of IpaH9.8, an inhibitor of GBPs, which also did not impact RNF213 expression (Fig. 4D), as anticipated. Functional and physical interaction of the effector IpaH2.5 with murine Rnf213 in intestinal tissue was further demonstrated using a UBAIT (Ubiquitin-Activated Interaction Traps) approach (Fig. S1). Collectively, these data demonstrate that the virulence factors IpaH1.4 and IpaH2.5 promote the degradation of mouse as well as human RNF213.

Loss of IpaH1.4 is sufficient to render *S. flexneri* susceptible to RNF213-driven ubiquitylation in human and murine host cells

Given that ectopic expression of either IpaH1.4 or IpaH2.5 was sufficient to degrade RNF213, we expected these two endogenous effectors to be functionally redundant. However, we found that genetic deletion of *ipaH1.4* in either *S. flexneri* serotype 2a strain 257T (Fig. 5A-B) or in serotype 5a strain M90T (Fig. S2) was sufficient to restore RNF213 protein expression and RNF213 recruitment to cytosolic bacteria. A deletion mutant of *ipaH2.5* was as resistant to RNF213 targeting as co-isogenic WT bacteria and a Δ*ipaH1.4-ipaH2.5* double mutant was indistinguishable from the Δ*ipaH1.4* single deletion mutant (Fig. S2). These data suggested that endogenous IpaH2.5 is non-functional, which agrees with a previous characterization of *ipaH2.5* as a minimally expressed pseudogene (36).

While infection of A549s with the Δ*ipaH1.4* mutant had no appreciable impact on RNF213 expression, *S. flexneri* Δ*mxiE* infections still led to a moderate reduction in RNF213 expression compared to uninfected (UI) cells (Fig. 5A). These data agree with previously published data that showed diminished but not abolished expression of IpaH proteins in Δ*mxiE* mutants (27, 37). As expected, a control infection with Δ*ipaH9.8*

reduced RNF213 expression in the same way as WT *S. flexneri* infections did (Fig. 5A). The sustained RNF213 expression in cells infected with *S. flexneri* Δ*ipaH1.4* (Fig. 5A) corelated with staining of cytosolic Δ*ipaH1.4* bacteria with RNF213 (Fig. 5B – C) as well as M1-, K27-, and K63-linked ubiquitin (Fig. 5D - G) in IFNγ-primed WT A549 cells. In contrast to IFNγ-primed WT A549 cells, IFNγ-primed RNF213^{KO} A549 cells lacked linear ubiquitylation of Δ*ipaH1.4* (Fig. 5E).

Although *S. flexneri* is a human-adapted pathogen, some IFNγ-inducible host defense programs targeting *S. flexneri* and the corresponding bacterial evasion mechanisms transcend host barriers. For example, the *Shigella* virulence factor IpaH9.8 inhibits both human and murine guanylate binding proteins (GBPs) (22, 38). We therefore asked whether RNF213 ubiquitylates *S. flexneri ΔipaH1.4* in at least one other mammalian species, the mouse. To do so, we infected unprimed and IFNγ-primed WT and Rnf213^{KO} mouse embryonic fibroblasts (MEFs, Fig. S3A) with *S. flexneri* WT and *ΔipaH1.4* mutant. We observed that *ΔipaH1.4* bacteria became decorated with mouse Rnf213 (Fig. S3B) and linear ubiquitin chains (Fig. S3C). Linear ubiquitin was present on *ΔipaH1.4 S. flexneri* in IFNγ-primed WT but not in *Rnf213*^{KO} MEFs (Fig. S3C). Collectively, these data depict a conserved role for the mammalian ubiquitin E3 ligase RNF213 in cytosolic immune surveillance and demonstrate that IpaH1.4 can evade both mouse and human RNF213-driven linear ubiquitylation.

Ubiquitylated microbial cargo can be delivered into microbicidal lysosomes in an autophagy-like process commonly referred to as xenophagy (39). Previous work showed that linear ubiquitylation of *S. enterica* leads to bacterial clearance by xenophagy (3). In contrast to the xenophagic killing of ubiquitylated *S. enterica,* we found that the ubiquitylated *S. flexneri ΔIpaH1.4* and *ΔmxiE* mutants continued to replicate inside of IFNγ-primed A549 cells (Fig. 5H), reminiscent of the continued growth of ubiquitylated *B. thailandensis tssM* mutants inside the host cell cytosol of human IFNγ-primed cells (9). Thus, our data indicate that *S. flexneri*, like *B. thailandensis,* can block ubiquitin-dependent xenophagy both at the stage of ubiquitylation and at another so far undetermined downstream step of this cell-autonomous host defense pathway.

DISCUSSION

Xenophagy is a cell-autonomous defense program in which intracellular pathogens are captured and delivered into degradative lysosomes. Ubiquitylation of intracellular pathogens is the most common initiating step for xenophagy (39). Like other steps of the xenophagy cascade, pathogen ubiquitylation is augmented in cells primed with the lymphocyte-derived cytokine IFNγ (2, 4, 7, 40, 41). An antimicrobial E3 ubiquitin ligase, RNF213, is itself an IFNγ-inducible protein (2-7). Here, we report that the enteric human pathogen *S. flexneri* employs the T3SS effector IpaH1.4 to induce the proteasomal degradation of RNF213. Accordingly, loss of IpaH1.4 results in RNF213-depdendent ubiquitylation of *S. flexneri*. However, IpaH1.4-deficient *S. flexneri* mutants, despite their ubiquitylation, continue to replicate inside the cytosol of IFNγ-primed human cells. These observations suggest that *S. flexneri* not only blocks RNF213-driven ubiquitylation but also the downstream degradation of ubiquitylated bacteria.

Accompanying previous reports on *Chlamydia* and *Burkholderia* (4, 9), our study on *Shigella* provides evidence that host-adapted intracellular escape from RNF213-driven host defense. Each of these pathogens evolved a mechanistically distinct strategy to escape ubiquitylation by RNF213. The soil-dwelling accidental pathogen *B. thailandensis* is recognized and ubiquitylated by RNF213 but instantly removes ubiquitin from its surface through the activity of its secreted ubiquitin esterase TssM (9). The human pathogen *Chlamydia trachomatis* decorates its surrounding vacuole with the secreted T3SS effector GarD, which renders the *Chlamydia*-containing vacuole invisible to RNF213 (4). In contrast to TssM and GarD, the *Shigella* effector IpaH1.4 is a direct inhibitor of RNF213.

IpaH1.4 and IpaH2.5 have nearly 99% sequence identity in their substrate-binding LRR and overexpression of either paralog is sufficient to trigger RNF213 degradation. However, only IpaH1.4 appears to be essential for *S. flexneri*-triggered RNF213 degradation – as shown in the present work – or for HOIP degradation (28). While these observations agree with a previous report demonstrating low expression of IpaH2.5 under standard culture conditions (36), it remains to be seen whether IpaH2.5 is expressed and possibly redundant with IpaH1.4 for virulence during *in vivo* infections.

The mechanism by which IpaH1.4 and its paralog IpaH2.5 promote RNF213 degradation can be gleaned from previous studies characterizing IpaH1.4 and IpaH2.5 as ubiquitin E3 ligases that directly conjugate K48-linked ubiquitin to the LUBAC subunit HOIP leading to HOIP degradation by the proteasome (28). We propose that IpaH1.4 and IpaH2.5 similarly bind to and directly ubiquitylate RNF213 to facilitate RNF213's proteasomal degradation. Such direct interactions are supported by our data showing that transient IpaH2.5-RNF213 interactions can be trapped via formation of covalent bonds between these proteins in a UBAIT assay. Future studies are needed to further probe for direct RNF213-IpaH1.4/IpaH2.5 interactions and to characterize the molecular structure of the protein binding interfaces.

The deletion of *ipaH1.4* leads to *S. flexneri* ubiquitylation in IFNγ-primed host cells. Different ubiquitin linkage types and their incorporation into heterotypic conjugates create a rich diversity of ubiquitin modifications with unique functional outputs, which is commonly referred to as the 'ubiquitin code.' (42, 43). We found that at least three linkage types are attached to *S. flexneri* Δ*ipaH1.4* in an RNF213-dependent manner: K27, K63, and linear (M1). Linear ubiquitylation is a head-to-tail inter-ubiquitin linkage through the amino group of the N-terminal methionine (M1) and the C-terminal carboxyl group (44). The LUBAC complex is the only recognized ubiquitin E3 ligase able to conjugate M1-linked ubiquitin chains (45, 46). However, we observed that LUBAC is dispensable for M1-linked ubiquitylation of cytosolic *S. flexneri* Δ*ipaH1.4.* We found that lysine-less internally tagged ubiquitin or an M1-specific antibody bound to *S. flexneri* Δ*ipaH1.4* in cells lacking LUBAC (HOIL-1^{KO} or HOIP^{KO}) but failed to bind bacteria in RNF213-deficient cells. These data corroborate our previous observations, which showed that IFNγ-induced linear ubiquitylation of *Chlamydia*- and *Toxoplasma*-containing vacuoles also occurs independent of LUBAC in human cells (2, 4). While it seems likely that RNF213 itself is the enzyme catalyzing linear ubiquitin conjugation, additional biochemical studies are needed to validate this hypothesis.

It was previously reported that RNF213 ubiquitylates LPS on the surface of *S. enterica* prompting the recruitment of LUBAC, which catalyzes the conjugation of linear ubiquitin to the surface of *S. enterica* (3). Whereas LUBAC was found to be essential for M1-linked ubiquitylation of cytosolic *S. enterica* (25), we find that LUBAC is dispensable

for M1-linked ubiquitylation of *S. flexneri* Δ*ipaH1.4* bacteria. While differences between *S. enterica* and *S. flexneri,* for example in the composition of their bacterial cell walls, could possibly contribute to these discrepant results, it is also important to note that the previous *S. enterica* infection studies were conducted in naïve cells (3, 25), whereas our studies were performed under IFNγ priming conditions. We therefore propose that a boost in the expression of RNF213 and other IFN-stimulated genes (ISGs) renders LUBAC obsolete for M1-linked ubiquitylation of Gram-negative bacteria. Future studies are needed to determine how RNF213 co-operates with LUBAC and other host factors to ubiquitin-tag intracellular pathogens.

Shigella is a human adapted pathogen that secretes T3SS effectors to directly interfere with type I and III IFN signaling in epithelial cells (47). Additionally, *Shigella* employs virulence factors that inhibits ISGs which act downstream from IFN signaling. For example, the T3SS effector IpaH9.8 blocks the activity of IFNγ-inducible antimicrobial ISGs such as GBP1 (19-22). Here we report that IpaH1.4 inactivates another ISG, *i.e.* RNF213. Because ubiquitylated *S. flexneri* Δ*ipaH1.4* and Δ*mxiE* mutants continue to replicate inside the cytosol of IFNγ-primed host cells, we propose that *S. flexneri* also uses a mxiE-independent T3SS effector to interfere with host defenses occurring downstream from RNF213. Collectively, these data indicate that *Shigella* is equipped with redundant counter-immune mechanisms. This type of bacterial effector redundancy is not unique to *Shigella*. It was recently shown that the rodent pathogen *Citrobacter rodentium* can tolerate various combinations of individual T3SS effector deletions *in vivo,* an observation that led to the 'T3SS effector networks' hypothesis (48, 49). Further characterization of the *Shigella* T3SS effector network that renders bacteria resistant to IFNγ-inducible cell-autonomous immune program will provide a deeper understanding of the pathogenesis of this important human enteric pathogen. Given the rise of extensively drug-resistant *Shigella* strains (50-53), such an understanding may prove to be essential for the development of critically needed novel therapeutic approaches to treat Shigellosis.

MATERIALS AND METHODS

Cell culture

A549 (ATCC #CCL-185), HT-29 (ATCC #HTB-38), and mouse embryonic fibroblasts (MEFs) were cultured in Dulbeco's Modified Eagle Medium (DMEM, Gibco) supplemented with 1% MEM non-essential aminoacids (Gibco), 55 uM 2-Mercaptoethanol (Gibco) and 10% heat inactivated fetal bovine-serum. MEFs were generated from E12- E14 embryos as previously described (54). Cells were grown at 37 °C in 5% $C0_2$. Cell lines were authenticated using GenePrint10 (Promega) by the Duke University DNA Analysis Facility. All cell lines were routinely tested for mycoplasma.

Knock out cell lines and mammalian expression systems

The production and characterization of A549 knockout cell lines (pooled RNF213KO, $HOIP^{KO}$ clone and $HOIL\text{-}1^{KO}$ clone) was previously reported (2, 4). Various GFP-tagged IpaH expression constructs including the IpaH1.4 and IpaH2.5 C/S mutants were previously described (28). Internally Strep-tagged ubiquitin (INT-Ub) open reading frames were cloned via Gateway cloning into the lentiviral expression plasmid pLEX307, a gift from Dr. David Root (Addgene plasmid # 41392; http://n2t.net/addgene:41392; RRID: Addgene_41392). DNA of full length human RNF213 with N-terminal mCherry was a gift from Daisuke Morito (55). RNF213 was amplified in segments using PCR and cloned using Golden Gate assembly with the enzyme kit BsmBI-v2 (New England Biolabs). Endogenous BsmBI sites were removed from RNF213 by introducing silent mutations in primers used to add enzyme overhangs for Golden Gate assembly. RNF213 was first cloned into a modified Gateway donor vector pDONR221 (Thermo Fisher Scientific) containing a golden gate cloning site in between ATTP sites to make pENTR-mCherry-RNF213. mCherry-RNF213 was transferred into piggybac vector PB-TA-ERN using LR clonase enzyme (Thermo Fisher Scientific) for dox-inducible expression of mCherry-RNF213. PB-TA-ERN (56) was a gift from Knut Woltjen (Addgene plasmid #80474; http://n2t.net/addgene:80474; RRID: Addgene_80474). Whole plasmid sequencing of PB-TA-ERN-mCherry-RNF213 and the INT-Ub vectors was performed by Plasmidsaurus using Oxford Nanopore Technology with custom analysis and annotation. The INT-Ub

protein sequences are provided in table 1 in supplemental material. For mCherry-RNF213 expression in human cells, 293T cells (ATCC CRL-3216) were transfected with PB-TA-ERN and piggybac transposase (pRP[Exp]-EGFP-EF1A>hyPBase, VectorBuilder) using lipofectamine 2000 transfection reagent (Thermo Fisher Scientific), according to manufacturer's instructions. Cells were grown for approximately 8 days to allow for loss of the transiently transfected vectors, while mCherry-RNF213 that had integrated into the 293T genome was being maintained.

Production of Rnf213 knockout mouse and derived cells

RNF213 knockout mice were generated using a modified iGONAD methodology (57-59). Briefly, 1-day time mated, vaginal-plug-positive 8 – 24-week-old C57BL/6J female mice were put under isoflurane anesthesia. A dorsal surgical incision was made, and the ovary/oviduct was exposed. The oviduct was injected with a 0.5 µL Cas9/CRISPR mix which included 6.1 µM Cas9 protein (IDT, Cat. #1081058), 30 µM sgRNAs (IDT, Alt-R CRISPR-Cas9 sgRNA), and 0.02% Fast Green FCF (VWR, Cat. #AAA16520-14) in Opti-MEM (Thermo Fisher Scientific, Cat. #11058021). The 30 µM sgRNA concentration included the following two sgRNAs targeting exon 28 of Rnf213: 5'-TTAAATACTGGTAAGGTCGT(TGG)-3' and 5'-AGTCGGAGTAGCAAAATCCC(TGG)-3'. After the Cas9/sgRNA mix injection, the oviducts were covered with tissue and then electroporated using a CUY21EDIT II (BEX Co., Ltd.) electroporator with the settings: Square mA mode, Pd V: 60 V, Pd A: 100 mA, Pd on: 5 ms, Pd off: 50 ms, Pd N: 3, and Decay: 10%. This procedure was done on both set of oviducts in the mouse. After surgery, female mice were housed together and at 19-21 days post-surgery monitored for pup birth. Pups were genotyped and three founder mice with out-of-frame 101 bp, 284 bp, or 407 bp deletions within exon 28, respectively, were selected and bred to homozygosity. Loss of Rnf213 protein expression in cells derived from these knockout mice was validated by Western blotting.

Lentivirus production

Plasmids were transfected into HEK293T cells using the TransIT 293 transfection reagent (Mirus). Wells were transfected with 1ug plasmid, 750 ng pGAGpol, 250 ng VSVG. 6

hours post transfection, media was aspirated and replaced with fresh DMEM. 24 hours post transfection, media was aspirated and replaced with pseudoparticle DMEM (3%fbs, 1% MEM non-essential aminoacids, 20mM HEPES). Supernatant was collected 48 and 72 hours after transfection. Supernatants containing lentivirus were filtered using 0.45um filters (corning) and later mixed with 10ug/ml polybrene (Millipore Sigma). Virus was frozen at -80 until use. For cell transduction, A549 cells were diluted to a concentration of 3.33 x 10^4 cells/ml and mixed with 10 ug/ml polybrene. 500 µl of lentivirus was added to each well of a 6 well plate, and 1.5 ml of diluted cells were added on top. Cells were selected in media with 1µg/ml of puromycin and expanded.

IpaH mini-screen

HEK293T that express PiggyBac RNF213 were seeded at 10^5 cells/well. Sixteen hours before transfection, ATc was added to cells to induce expression of RNF213. The next morning, 2.5 µg of IpaH effector encoding plasmids were used to transfect HEK293T using the TransIT 293 transfection reagent (Mirus). 24 hours after transfection, cells were lysed in RIPA buffer and prepared for immunoblotting.

Bacterial strains

All *S. flexneri* strains were grown on Tryptic Soy Broth (TSB, Millipore Sigma) agar plates in presence of 0.01% of Congo Red (Millipore Sigma) and red colonies were cultured in TSB broth culture. *S. flexneri* 2457T wildtype and mutant strains (*ΔmxiE and ΔipaH1.4*) were previously described (19). *S. flexneri* M90T strains (wildtype, *ΔipaH2.5, ΔipaH1.4 and* ∆*ipaH1.4-ipaH2.5*) were also previously reported (28). For immunofluorescence studies, we used fluorescent *S. flexneri* strains carrying the pGFPmut2 plasmid (60). Bacteria were transformed with the ilux pGEX(-) plasmid (Addgene plasmid #107879) (61) to generate bioluminescent bacteria, as previously reported (62). Where specified, *S. flexneri*. strains were used that harbor the pilT plasmid which encodes an adhesin (63) and enhances bacterial adhesion to host cells. Antibiotics were used as needed at the following concentration: carbenicillin (50 ug/ml), kanamycin (50 ug/ml), and chloramphenicol (100 ug/ml).

Infection procedures

For immunofluorescence staining A549, HT29, and MEF cells were seeded at $1x10^5$ cells per well on cover slips in 24-well plates. HT29 cells were plated at $2x10^5$ cells per well. For Western blotting cells were plated at $2x10^5$ cells per well in 24-well plates. Cells were either left untreated or treated overnight with human or mouse cytokine IFNγ at a final concentration of 100 U/ml, as indicated. The day before infection, *S. flexneri* was inoculated into TSB with antibiotics as needed and grown overnight at 37°C with aeration. The next day bacteria were diluted (1:20) in TSB with antibiotics and grown for 1h 30 minutes. Subsequently, the optical density of the broth culture was measured and pelleted bacteria were washed in sterile PBS and resuspended in DMEM. Infections were carried out at an approximate multiplicity of infection (MOI) of 50 to 100, unless otherwise specified. Cells were centrifuged at 1000 g for 10 minutes at the time of infection and infected cells were incubated at 37°C with 5% CO_2. Cells were washed with warm HBSS two times after 90 minutes (A549 and HT29 cells) or 60 minutes (MEFs) post infection. Following these washes gentamicin at a final concentration of 50 ug/ml (for A549 and MEFs) or 100 ug/ml (for HT29) was added to the media. For fluorescence microscopy infected cells were fixed with 4%PFA in phosphate-buffered saline (PBS) at 4 hpi (A549 cells), 3 hpi (HT29), or 2 hpi (MEFs). All *S. flexneri* strains carried the plasmid pGFPmut2 to visualize bacteria by fluorescence microscopy. For Western blotting, bioluminescence experiments, and MEF infections, *S. flexneri* strains expressed PilT for improved adhesion and infection rates.

Immunofluorescence microscopy

Cells were fixed in 4% PFA in PBS and then permeabilized either with 0.1%triton in PBS for 15 minutes or with ice-cold methanol for 1 minute followed by 0.05% saponin in blocking buffer. Blocking buffer was composed of 5% BSA, 2.2% glycine +/- 0.05% saponin or 10% goat serum and 0.05 % saponin in PBS. Following permeabilization, coverslips were blocked for 30 minutes at room temperature (RT). Next, coverslips were incubated with the respective primary antibody diluted in blocking buffer overnight at 4°C. The following primary antibodies were used: rabbit monoclonal anti-RNF213 (Sigma HPA026790; 1:1000), rabbit monoclonal anti-linear (M1) ubiquitin; clone 1E3 (Sigma

ZRB2114; 1:250), mouse polyclonal anti-ubiquitin FK2 (Cayman Chemical 14220; 1:100), rabbit monoclonal anti-K63 ubiquitin, clone Apu3 (Sigma 05-1308. 1:100), rabbit monoclonal anti K27 (Abcam ab181537, 1:100), mouse monoclonal anti-Strep (Genscript A01732, 1:200), custom rabbit anti-mRnf213 antibody from an animal immunized with peptides RKSNEGGNTQPEDQRKPGEGR (aa296-316) and KDTVEYEFIYEQAQKKGE (aa429-446) (Life Technologies, 1:100). Coverslips were then washed three times with 0.05% Triton in PBS or 0.05% saponin and incubated with an Alexa Fluor-conjugated secondary antibody (1:1000, Invitrogen) and nuclear dye Hoechst 33258 (2ug/ml; Invitrogen) for 1 hour at RT. Next, coverslips were washed three times with 0.05% Triton or 0.05% saponin in PBS and mounted on glass slides using a mix of with mowiol 4-88 combined with para-phenylenediamine antifading agent (9:1). Coverslips were imaged at a Zeiss Axio Imager microscope with Apotome 3 using a 63×/1.4 NA Oil immersion lens. Two to eleven fields of view were captured per coverslip to account for at least 100 bacteria, and z slices with an interval of 0.5 µm were taken per field of view. Images were processed on the software program Fiji. Bacteria that had protein signal surrounding at least 50% of its visible surface were considered as targeted.

Bacterial luminescence assay

Infections were conducted with bacterial strains carrying the pilT plasmid to promote cell adhesion and the ilux plasmid as a bioluminescence reporter. Host cells were seeded in 96-well plates at a density of 2.5 x10^4 cells per well. An approximate MOI of 5 in an infection volume of 100 µl per well was used. Twenty-five minutes post infection, wells were washed once with 200 µl of warm HBSS and then fresh DMEM containing 50µg /ml gentamicin was added to each well. Bacterial bioluminescence was measured on a multimode microplate reader (Biotek Synergy H1, Agilent) every 30 minutes, starting at 1 hpi and finishing at 8 hpi.

Western blotting

After infection, cells were washed two times with cold HBSS and lysed in RIPA buffer (Sigma) in the presence of 4U/ml DNAse I (NEB) and protease inhibitor cocktail (Sigma). Lysates were incubated at 4°C for 30 min and centrifuged at 20,000g for 12 minutes at

4°C. Protein concentrations were measured using the BCA kit (Thermofisher) and normalized. Normalized samples were mixed with Laemmli buffer that contained 5% β-mercaptoethanol and heated at 95°C for 10 minutes. Sample were heated at 56 °C for 10 minutes when samples were prepared for RNF213 immunoblotting. Ten to thirty µg of protein sample were resolved on a 4-20% Mini-Protean TGX stain-free gels (Biorad) and then blotted onto a PVDF membrane using a tank transfer system overnight at 4°C. After the transfer, PVDF membranes were blocked with 5% nonfat dry milk in Tris-buffered saline containing 0.1%Tween20 (Sigma-Aldrich) (TBS-T) for 1 hour at RT. Subsequently, membranes were incubated with primary antibody diluted in blocking solution overnight at 4°C. After primary antibody incubation, blots were washed three times with TBST and incubated with the respective secondary antibody in blocking solution for 1 hour at RT. Afterwards, membranes were washed with TBS-T and developed with Clarity ECL (Cytiva). Blots were imaged on an Azure 500 visualization system. Primary antibodies used in this study include rabbit monoclonal anti-RNF213 (Sigma HPA026790 1:2000), rabbit polyclonal anti-GAPDH (Abcam ab9845; 1:10000); mouse monoclonal anti HOIL-1, clone E3E (Sigma MABC576; 1:500); custom rabbit anti-mRnf213 (Life Technologies, 1:500); rabbit polyclonal anti-HOIP (Abcam ab46322; 1:500); monoclonal Anti-β-Actin (Sigma A2228, 1:6000). Images were processed in Fiji.

UBAIT Substrate Capture Assays.

UBAIT assays were performed essentially as described before (32). Briefly, unknown substrates were captured from colon and cecum lysates from 6-8 weeks old wild type C57BL/6 (Charles River) mice. All mouse infection experiments conducted were in accordance with the policies of the Institutional Animal Care and Use Committee at UT Southwestern. Mice were orally infected by gavage with $1x10^9$ *Salmonella enterica* Typhimurium S1344 WT and after 4 days mice were euthanized and colon and cecum were removed, washed and homogenized in Lysis Buffer (1x Ubiquitination buffer (Boston Biochem), 1x protease inhibitor (Sigma), 1mM DTT). Homogenates were then centrifuged at 13,000g at 4˚C for 10 minutes and supernatants were added to UBAIT reactions. The supernatant were incubated with 25 ug of purified Strep-IpaH2.5-3xFLAG-Ub or Strep-IpaH3-3xFLAG-Ub and rotated at 4˚C. After 1 hour, His-UbE1 (100nM), His-UbcH5b

(2000nM), energy regeneration buffer (Boston Biochem), MgCl (1mM) and 1 x ubiquitination buffer were added to a final volume of 500 µl. The reaction was run at 30˚C for 10 minutes and then 300 µl TBS buffer (25 mM Tris-HCL pH7.4, 150 mM NaCl, 1mM DTT) and 30 µl of washed Strep-Tactin Superflow beads (Iba LifeSciences) were added and rotated for 2 hours at 4˚C. The beads were washed 4 times in TBS-T (TBS+ 0.5% Triton-X100) and 2 times in TBS. Strep-IpaH2.5-3xFLAG-Ub was eluted from the beads in 150 µl Strep-tag elution buffer (Iba LifeSciences). Eluted sample and beads were centrifuged, and supernatant moved to a new tube. SDS (0.25% final concentration) and DTT (5mM final concentration) were added, and samples were heated at 95˚C for 5 minutes. Next, 1.2 ml TBS was added, followed by 20 µl of M2-FLAG beads (Sigma). The mixture was rotated for 2 hours at 4˚C. M2-FLAG beads were washed 4 times in TBS-T followed by 2 times in TBS. Finally, 35 µl of hot (95˚C) SDS-PAGE Loading Buffer was added and the beads were heated for an additional 5 minutes at 95˚C. Samples were electrophoresed on a gradient precast SDS-PAGE gel (Biorad) and Coomassie stained. A lane of gel above the band with unmodified Strep-IpaH2.5-3xFLAG-Ub or Strep-IpaH3-3xFLAG-Ub was excised, and proteins were digested overnight with trypsin (Pierce) following reduction and alkylation with DTT and iodoacetamide (Sigma–Aldrich). Following solid-phase extraction cleanup with an Oasis HLB µelution plate (Waters), the resulting peptides were reconstituted in 10 µL of 2% (v/v) acetonitrile (ACN) and 0.1% trifluoroacetic acid in water. Two µL of each sample were injected onto an Orbitrap Fusion Lumos (Thermo) mass spectrometer, coupled to an Ultimate 3000 RSLC-Nano liquid chromatography systems (Thermo) at the Mass Spectrometry Core at University of Texas Southwestern. Samples were injected onto a 75 µm i.d., 75-cm long, (Lumos) EasySpray column (Thermo), and eluted with a gradient from 0-28% buffer B over 90 minutes. Buffer A contained 2% (v/v) ACN and 0.1% formic acid in water, and buffer B contained 80% (v/v) ACN, 10% (v/v) trifluoroethanol, and 0.1% formic acid in water. The Orbitrap Fusion Lumos mass spectrometer operated in positive ion mode with a source voltage of 2.0-2.4 kV and an ion transfer tube temperature of 275 °C. MS scans were acquired at 120,000 resolution in the Orbitrap and up to 10 MS/MS spectra were obtained in the Orbitrap for each full spectrum acquired using higher-energy collisional dissociation (HCD) for ions with charges 2-7. Dynamic exclusion was set for 25 seconds after an ion was selected

for fragmentation. Raw MS data files were analyzed using Proteome Discoverer v.2.4 (Thermo), with peptide identification performed using Sequest HT searching against the human reviewed protein database from UniProt. Fragment and precursor tolerances of 10 ppm and 0.6 Da (Lumos) was specified, and three missed cleavages were allowed. Carbamidomethylation of Cys was set as a fixed modification and oxidation of Met was set as a variable modification. The false-discovery rate (FDR) cutoff was 1% for all peptides. The abundance of identified peptides found for Strep-IpaH2.5 UBAIT were compared to those found for control IpaH3 UBAIT that was included in the same experiment. Hits for IpaH2.5 were included when abundance levels were at least 2-fold higher than UBAIT controls.

Statistical analysis

Graphpad Prism 10.2.2 was used to generate graphs and to perform statistical analyzes. Experiments were conducted in three to five biological replicates. Data in graphs are displayed as mean ± standard error of the mean (SEM). Statistical analyses included student t-test one-way and two-way analysis of variance (ANOVA) followed by Tukey's multiple comparison tests. Significance was considered when p values were <0.05

Data storage

Mass spectrometry data (Ubait) will be deposited in a publishably accessible Repository at the University of Texas Southwestern at the time at which the final version of the manuscript is published. The numerical values of all other quantified data depicted in data panels in this manuscript will be made openly available in the Digital Repositories at Duke at the time at which the final version of the manuscript is published. Digital object identifier will be provided.

ACKNOWLEDGEMENTS

This work was supported by National Institutes of Health grants AI139425 (to JC), AI083359 (to NMA), AI137031 (to NSH), and AI168107 (to NSH); and the Welch Foundation (grant I-1704 to NMA). NSH holds an Investigators in the Pathogenesis of Infectious Disease Award from the Burroughs Wellcome Fund. The funders had no role in study design, data collection and interpretation, or the decision to submit the work for publication. We would like to thank members of the Coers lab as well as the labs of Drs. Clare Smith, David Tobin, and Edward Miao for providing valuable feedback.

FIGURE LEGENDS

Fig. 1. Mutation of the bacterial transcription factor MxiE results in linear ubiquitylation of *S. flexneri* in IFNγ-primed epithelial cells. (A - C) Cells were primed with 100 U/ml IFNγ or left unprimed and then infected with WT or *ΔmxiE S. flexneri* at an MOI of 50 - 100. Cells were fixed 3 - 4 h post infection (hpi) and stained for linear ubiquitin (M1-Ub) with anti-M1 antibody. Percentage of M1-Ub-positive bacteria was quantified in infected A549 epithelial cells at 4 hpi **(B)** and HT29 epithelial cells at 3 hpi **(C)**. Graphs show the average of three independent experiments and depict means ± SEM. Two-way ANOVA with Tukey's multiple comparison tests were performed; all statistically significant comparisons are shown. ***$p<0.001$; **** $p<0.0001$; ns, not significant

Fig. 2. *S. flexneri* Δ*mxiE* mutants become decorated with linear and lysine-linked ubiquitin in IFNγ-primed A549 cells. (A) WT A549 cells expressing the indicated internally Strep-tagged Ubiquitin (INT-Ub) variants were primed with 100 U/ml IFNγ overnight and co-localization of INT-Ub with cytosolic *S. flexneri* (Sf) Δ*mxiE* was assessed at 4 hpi. Ubiquitin linkage-specific antibodies were used to determine the percentage of *S. flexneri* Δ*mxiE* staining positive for K27-linked ubiquitin (K27-Ub) **(B)** or K63-linked ubiquitin **(C)** in IFNγ-primed untransduced WT A549 cells. Co-staining of anti-M1 and anti-ubiquitin (FK2) on the surface of *S. flexneri* Δ*mxiE* in IFNγ-primed (100U/ml) A549 cells is shown in (D). Quantification of anti-M1-FK2 co-staining in untreated and IFNγ-primed A549 cells is depicted in (E). All infections were done at an MOI of 50 - 100. Data was generated from at least three independent experiments and shows mean ± SEM. One-way ANOVA followed by Dunnet's multiple comparisons were performed of all groups against WT-ubiquitin group **(A)**. Two-way ANOVA with Tukey's multiple comparison tests were performed for **(B)** and **(C)**. An unpaired t-test was performed between "both FK2+M1" groups (gray bars) (**E).** *$p<0.05$; **$p<0.01$; ***$p<0.001$; **** $p<0.0001$

Fig. 3 Ubiquitylation of *S.flexneri ΔmxiE* is dependent on RNF213 but not LUBAC **(A)** Immunoblotting for HOIP, HOIL-1, and RNF213 protein expression in untreated and IFNγ-primed WT and the corresponding gene deletion (KO) A549 cells. **(B)** Percentage of M1-linked ubiquitin positive Δ*mxiE S.flexneri* in IFNγ-primed WT, HOIP^{KO}, HOIL-1^{KO} and RNF213^{KO} A549 cells. **(C)** Percentage of WT and 7KR INT-Ub-positive Δ*mxiE S. flexneri* in IFNγ-primed WT, HOIP^{KO}, and RNF213^{KO} A549 cells. **(D – F)** Untreated and IFNγ-primed A549 and HT29 cells were infected with the indicated *S. flexneri* strains and immuno-stained for RNF213 and ubiquitin (FK2). Representative immunofluorescence microscopy images are shown for A549 infections in **(E).** RNF213-*S. flexneri* colocalization percentages were quantified in A549 **(D)** and HT29 **(F)** cells. **(G)** Quantification of ubiquitin and RNF213 colocalization with Δ*mxiE S. flexneri* in A549 cells. Percentages of Δ*mxiE S. flexneri* staining positive for antibodies specific for K27-linked **(H)** and K63-linked ubiquitin **(I)** are also provided. All data are represented by the mean ± SEM from at least three independent experiments. One-way ANOVA followed by Dunnet's multiple comparisons were performed of all groups against WT A549 group in **(A)**. Two-way ANOVA with Tukey's multiple comparison tests were performed in **(C, D** and **F)**. an unpaired t-test was performed between "both Ub+RNF213" groups (gray bars) in **(G)**. For **(H** and **I)**, an unpaired-t test was performed. **p<0.01;; **** p<0.0001

Fig. 4. *S. flexneri* virulence factors IpaH1.4 and IpaH2.5 induce proteasomal degradation of RNF213 (A-B) All *S. flexneri* strains express PilT to enhance adhesion and infection rates and infections were carried out at an MOI of 5 - 25 for 3 hours **(A)** Untreated and IFNγ-primed (100 U/ml) A549 cells were infected with indicated *S. flexneri* strains and protein lysates were probed for RNF213 expression. **(B)** Infected and uninfected A549 cells were cultured in the presence of different concentrations of the proteasomal inhibitor MG132 and RNF213 expression was monitored by immunoblotting. **(C)** HEK293T cells stably expressing mCherry-RNF213 were transiently transfected with individual GFP-tagged IpaH effectors for 24 hours and RNF213 expression was assessed. **(D)** WT and catalytically inactive C368S mutants of IpaH1.4 and IpaH2.5 were transiently transfected into HEK293T cells expressing mCherry-RNF213 and cell lysates were subjected to immunoblotting. **(C-D)** Denaturation of cell lysates at lower temperature

(56°C) was required for RNF213 detection but also resulted in the formation of double bands for all IpaH-GFP constructs. Images are representative of three independent experiments UI: Uninfected.

Fig. 5. Loss of IpaH1.4 is sufficient to render *S. flexneri* susceptible to RNF213-driven ubiquitylation (A) IFNγ-primed A549 cells were infected with the indicated PilT^{+} *S. flexneri* strains for 3 hours at an MOI of 5 - 25 and RNF213 protein levels were assessed by Western blotting. **(B)** Representative microscopy image depicting RNF213 recruitment to cytosolic Δ*IpaH1.4* bacteria in IFNγ-primed A549 cells. **(C)** Percentage of RNF213^{+} WT and Δ*IpaH1.4 S. flexneri* in IFNγ-primed A549 cells. **(D)** Representative microscopy image showing Δ*IpaH1.4 S. flexneri* decorated with M1-linked ubiquitin in IFNγ-primed A549 cells. Percentage of M1-linked **(E)**, K27-linked **(F)**, and K63-linked **(G)** ubiquitin-positive WT and Δ*IpaH1.4 S. flexneri* in IFNγ-primed WT **(E-G)** and RNF213^{KO} **(E)** A549 cells. **(H)** The ilux operon was introduced into *S. flexneri* strains to use bioluminescence (RLU) as a proxy for bacterial growth. RLU was measured in IFNγ-primed WT A549 cells infected with the indicated *S. flexneri* strains at an MOI of 5. **(C, F-H)** Data represent the mean ± SEM from at least three independent experiments. An unpaired t-test was conducted for **(C, F, G)**. One-way ANOVA followed by Dunnet's multiple comparisons were performed between all groups against the group of WT A549 cells **(E).** *p<0.05; ***p<0.001; **** p<0.0001

REFERENCES

1. J. L. Casanova, J. D. MacMicking, C. F. Nathan, Interferon-gamma and infectious diseases: Lessons and prospects. *Science* **384**, eadl2016 (2024).
2. D. Hernandez, S. Walsh, L. Saavedra Sanchez, M. S. Dickinson, J. Coers, Interferon-Inducible E3 Ligase RNF213 Facilitates Host-Protective Linear and K63-Linked Ubiquitylation of Toxoplasma gondii Parasitophorous Vacuoles. *mBio* 10.1128/mbio.01888-22, e0188822 (2022).
3. E. G. Otten *et al.*, Ubiquitylation of lipopolysaccharide by RNF213 during bacterial infection. *Nature* **594**, 111-116 (2021).
4. S. C. Walsh *et al.*, The bacterial effector GarD shields Chlamydia trachomatis inclusions from RNF213-mediated ubiquitylation and destruction. *Cell Host Microbe* 10.1016/j.chom.2022.08.008 (2022).
5. D. Houzelstein *et al.*, The ring finger protein 213 gene (Rnf213) contributes to Rift Valley fever resistance in mice. *Mamm Genome* **32**, 30-37 (2021).
6. F. Thery *et al.*, Ring finger protein 213 assembles into a sensor for ISGylated proteins with antimicrobial activity. *Nat Commun* **12**, 5772 (2021).
7. S. K. Matta *et al.*, Genome-wide and targeted CRISPR screens identify RNF213 as a mediator of interferon gamma-dependent pathogen restriction in human cells. *Proc Natl Acad Sci U S A* **121**, e2315865120 (2024).
8. L. Martina *et al.*, Proteome Profiling of RNF213 Depleted Cells Reveals Nitric Oxide Regulator DDAH1 Antilisterial Activity. *Frontiers in cellular and infection microbiology* **11**, 735416 (2021).
9. M. Szczesna *et al.*, Bacterial esterases reverse lipopolysaccharide ubiquitylation to block host immunity. *Cell Host Microbe* **32**, 913-924 e917 (2024).
10. C. Troeger *et al.*, Global disability-adjusted life-year estimates of long-term health burden and undernutrition attributable to diarrhoeal diseases in children younger than 5 years. *Lancet Glob Health* **6**, e255-e269 (2018).
11. T. E. Libby *et al.*, Consequences of Shigella infection in young children: a systematic review. *Int J Infect Dis* **129**, 78-95 (2023).
12. K. H. Bagamian, J. D. Anderson Iv, G. Blohm, S. Scheele, Shigella and childhood stunting: Evidence, gaps, and future research directions. *PLoS Negl Trop Dis* **17**, e0011475 (2023).
13. N. Mellouk, J. Enninga, Cytosolic Access of Intracellular Bacterial Pathogens: The Shigella Paradigm. *Frontiers in cellular and infection microbiology* **6**, 35 (2016).
14. M. M. Levine, K. L. Kotloff, E. M. Barry, M. F. Pasetti, M. B. Sztein, Clinical trials of Shigella vaccines: two steps forward and one step back on a long, hard road. *Nat Rev Microbiol* **5**, 540-553 (2007).
15. R. Raqib *et al.*, Persistence of local cytokine production in shigellosis in acute and convalescent stages. *Infect Immun* **63**, 289-296 (1995).
16. R. Raqib, B. Wretlind, J. Andersson, A. A. Lindberg, Cytokine secretion in acute shigellosis is correlated to disease activity and directed more to stool than to plasma. *J Infect Dis* **171**, 376-384 (1995).
17. M. Kutsch, C. Gonzalez-Prieto, J. Coers, The GBP1 microcapsule interferes with IcsA-dependent septin cage assembly around Shigella flexneri. *Pathog Dis* **79** (2021).

18. M. Kutsch *et al.*, Direct binding of polymeric GBP1 to LPS disrupts bacterial cell envelope functions. *EMBO J* **39**, e104926 (2020).
19. A. S. Piro *et al.*, Detection of Cytosolic Shigella flexneri via a C-Terminal Triple-Arginine Motif of GBP1 Inhibits Actin-Based Motility. *mBio* **8** (2017).
20. M. P. Wandel *et al.*, GBPs Inhibit Motility of Shigella flexneri but Are Targeted for Degradation by the Bacterial Ubiquitin Ligase IpaH9.8. *Cell Host Microbe* **22**, 507-518 e505 (2017).
21. L. Goers *et al.*, Shigella IpaH9.8 limits GBP1-dependent LPS release from intracytosolic bacteria to suppress caspase-4 activation. *Proc Natl Acad Sci U S A* **120**, e2218469120 (2023).
22. P. Li *et al.*, Ubiquitination and degradation of GBPs by a Shigella effector to suppress host defence. *Nature* (2017).
23. A. Bullones-Bolanos, J. Bernal-Bayard, F. Ramos-Morales, The NEL Family of Bacterial E3 Ubiquitin Ligases. *Int J Mol Sci* **23** (2022).
24. P. Schnupf, P. J. Sansonetti, Shigella Pathogenesis: New Insights through Advanced Methodologies. *Microbiol Spectr* **7** (2019).
25. J. Noad *et al.*, LUBAC-synthesized linear ubiquitin chains restrict cytosol-invading bacteria by activating autophagy and NF-kappaB. *Nat Microbiol* **2**, 17063 (2017).
26. C. D. Kane, R. Schuch, W. A. Day, Jr., A. T. Maurelli, MxiE regulates intracellular expression of factors secreted by the Shigella flexneri 2a type III secretion system. *J Bacteriol* **184**, 4409-4419 (2002).
27. M. Mavris, P. J. Sansonetti, C. Parsot, Identification of the cis-acting site involved in activation of promoters regulated by activity of the type III secretion apparatus in Shigella flexneri. *J Bacteriol* **184**, 6751-6759 (2002).
28. M. F. de Jong, Z. Liu, D. Chen, N. M. Alto, Shigella flexneri suppresses NF-kappaB activation by inhibiting linear ubiquitin chain ligation. *Nat Microbiol* **1**, 16084 (2016).
29. J. Liu *et al.*, Mechanistic insights into the subversion of the linear ubiquitin chain assembly complex by the E3 ligase IpaH1.4 of Shigella flexneri. *Proc Natl Acad Sci U S A* **119**, e2116776119 (2022).
30. K. Hiragi *et al.*, Structural insight into the recognition of the linear ubiquitin assembly complex by Shigella E3 ligase IpaH1.4/2.5. *J Biochem* **173**, 317-326 (2023).
31. G. Luchetti *et al.*, Shigella ubiquitin ligase IpaH7.8 targets gasdermin D for degradation to prevent pyroptosis and enable infection. *Cell Host Microbe* **29**, 1521-1530 e1510 (2021).
32. J. M. Hansen *et al.*, Pathogenic ubiquitination of GSDMB inhibits NK cell bactericidal functions. *Cell* **184**, 3178-3191 e3118 (2021).
33. R. Otsubo *et al.*, Shigella effector IpaH4.5 targets 19S regulatory particle subunit RPN13 in the 26S proteasome to dampen cytotoxic T lymphocyte activation. *Cell Microbiol* **21**, e12974 (2019).
34. J. R. Rohde, A. Breitkreutz, A. Chenal, P. J. Sansonetti, C. Parsot, Type III secretion effectors of the IpaH family are E3 ubiquitin ligases. *Cell Host Microbe* **1**, 77-83 (2007).
35. H. Ashida *et al.*, A bacterial E3 ubiquitin ligase IpaH9.8 targets NEMO/IKKgamma to dampen the host NF-kappaB-mediated inflammatory response. *Nat Cell Biol* **12**, 66-73; sup pp 61-69 (2010).

36. N. Silue, E. Marcantonio, F. X. Campbell-Valois, RNA-Seq analysis of the T3SA regulon in Shigella flexneri reveals two new chromosomal genes upregulated in the on-state. *Methods* **176**, 71-81 (2020).
37. A. Botteaux, M. P. Sory, L. Biskri, C. Parsot, A. Allaoui, MxiC is secreted by and controls the substrate specificity of the Shigella flexneri type III secretion apparatus. *Mol Microbiol* **71**, 449-460 (2009).
38. C. Ji *et al.*, Structural mechanism for guanylate-binding proteins (GBPs) targeting by the Shigella E3 ligase IpaH9.8. *PLoS Pathog* **15**, e1007876 (2019).
39. I. Tripathi-Giesgen, C. Behrends, A. F. Alpi, The ubiquitin ligation machinery in the defense against bacterial pathogens. *EMBO Rep* **22**, e52864 (2021).
40. A. K. Haldar *et al.*, Ubiquitin systems mark pathogen-containing vacuoles as targets for host defense by guanylate binding proteins. *Proc Natl Acad Sci U S A* **112**, E5628-5637 (2015).
41. M. C. Fernandez *et al.*, CT135 mediates the resistance of Chlamydia trachomatis to primate interferon gamma stimulated immune defenses. *iScience* **27**, 110143 (2024).
42. D. Komander, M. Rape, The ubiquitin code. *Annual review of biochemistry* **81**, 203-229 (2012).
43. I. Dikic, B. A. Schulman, An expanded lexicon for the ubiquitin code. *Nature reviews. Molecular cell biology* **24**, 273-287 (2023).
44. T. Kirisako *et al.*, A ubiquitin ligase complex assembles linear polyubiquitin chains. *EMBO J* **25**, 4877-4887 (2006).
45. K. Sasaki, K. Iwai, LUBAC-mediated linear ubiquitination in tissue homeostasis and disease. *J Biochem* **174**, 99-107 (2023).
46. L. Gao *et al.*, The mechanism of linear ubiquitination in regulating cell death and correlative diseases. *Cell death & disease* **14**, 659 (2023).
47. N. Alphonse *et al.*, A family of conserved bacterial virulence factors dampens interferon responses by blocking calcium signaling. *Cell* **185**, 2354-2369 e2317 (2022).
48. D. Ruano-Gallego *et al.*, Type III secretion system effectors form robust and flexible intracellular virulence networks. *Science* **371** (2021).
49. J. Sanchez-Garrido, D. Ruano-Gallego, J. S. Choudhary, G. Frankel, The type III secretion system effector network hypothesis. *Trends Microbiol* **30**, 524-533 (2022).
50. C. S. Tsai *et al.*, Shigellosis in Taiwan: An old enteric pathogen with changing epidemiology and increasing antimicrobial resistance. *J Microbiol Immunol Infect* **57**, 346-353 (2024).
51. E. S. Donkor, A. Odoom, A. H. Osman, S. Darkwah, F. C. N. Kotey, A Systematic Review on Antimicrobial Resistance in Ghana from a One Health Perspective. *Antibiotics (Basel)* **13** (2024).
52. X. M. Matanza, A. Clements, Pathogenicity and virulence of Shigella sonnei: A highly drug-resistant pathogen of increasing prevalence. *Virulence* **14**, 2280838 (2023).
53. H. O'Flanagan, M. Siddiq, C. Llewellyn, D. Richardson, Antimicrobial resistance in sexually transmitted Shigella in men who have sex with men: A systematic review. *Int J STD AIDS* **34**, 374-384 (2023).
54. J. Coers *et al.*, Chlamydia muridarum evades growth restriction by the IFN-gamma-inducible host resistance factor Irgb10. *J Immunol* **180**, 6237-6245 (2008).

55. M. Sugihara *et al.*, The AAA+ ATPase/ubiquitin ligase mysterin stabilizes cytoplasmic lipid droplets. *J Cell Biol* **218**, 949-960 (2019).
56. S. I. Kim *et al.*, Inducible Transgene Expression in Human iPS Cells Using Versatile All-in-One piggyBac Transposons. *Methods Mol Biol* **1357**, 111-131 (2016).
57. S. Skavicus, N. S. Heaton, Approaches for timeline reductions in pathogenesis studies using genetically modified mice. *Microbiol Spectr* **11**, e0252123 (2023).
58. C. B. Gurumurthy *et al.*, Creation of CRISPR-based germline-genome-engineered mice without ex vivo handling of zygotes by i-GONAD. *Nature protocols* **14**, 2452-2482 (2019).
59. M. Ohtsuka *et al.*, i-GONAD: a robust method for in situ germline genome engineering using CRISPR nucleases. *Genome Biol* **19**, 25 (2018).
60. B. P. Cormack, R. H. Valdivia, S. Falkow, FACS-optimized mutants of the green fluorescent protein (GFP). *Gene* **173**, 33-38 (1996).
61. C. Gregor, K. C. Gwosch, S. J. Sahl, S. W. Hell, Strongly enhanced bacterial bioluminescence with the ilux operon for single-cell imaging. *Proc Natl Acad Sci U S A* **115**, 962-967 (2018).
62. M. S. Dickinson *et al.*, LPS-aggregating proteins GBP1 and GBP2 are each sufficient to enhance caspase-4 activation both in cellulo and in vitro. *Proc Natl Acad Sci U S A* **120**, e2216028120 (2023).
63. P. Clerc, P. J. Sansonetti, Entry of Shigella flexneri into HeLa cells: evidence for directed phagocytosis involving actin polymerization and myosin accumulation. *Infect Immun* **55**, 2681-2688. (1987).

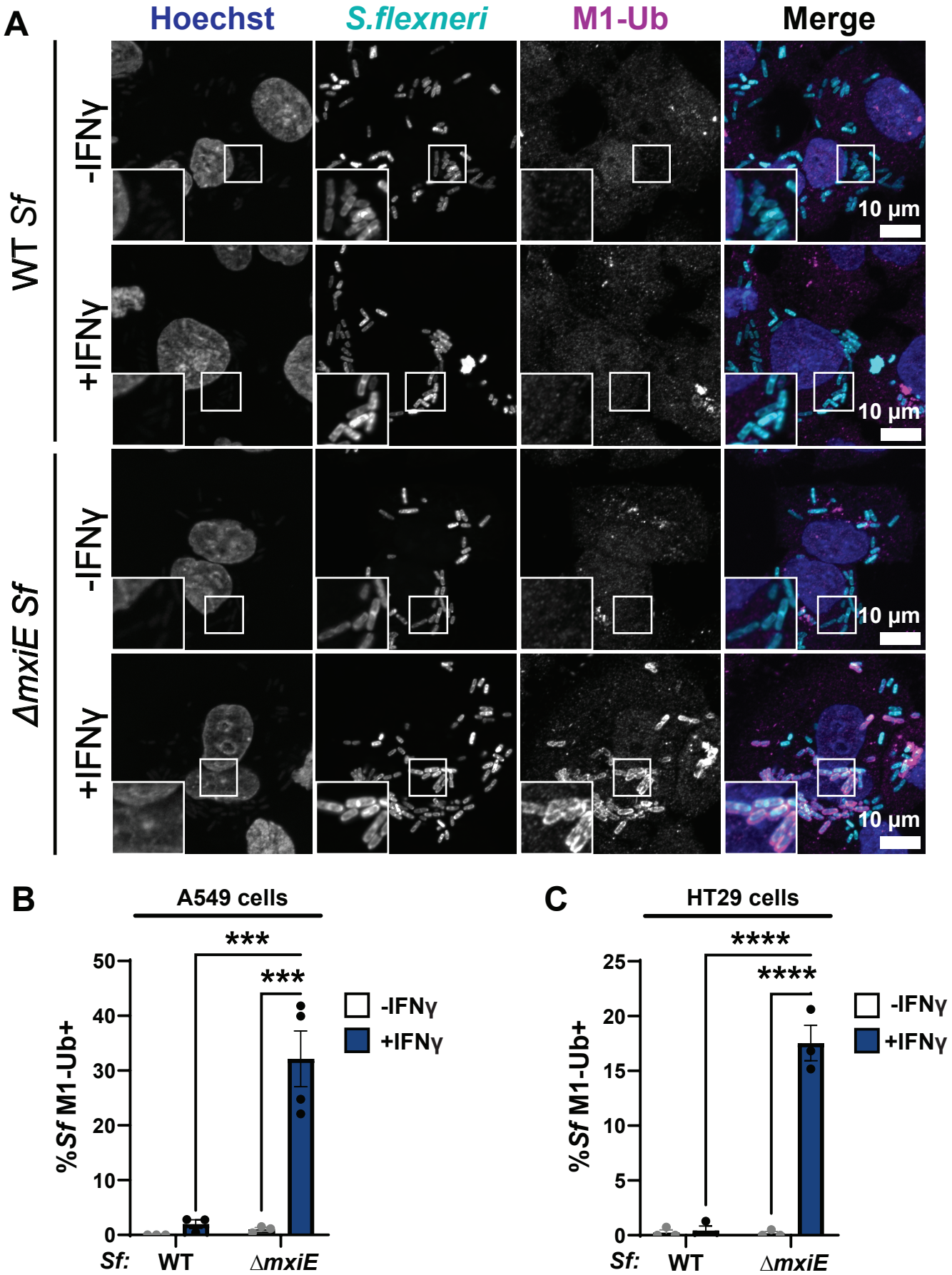
A
Hoechst
S.flexneri
M1-Ub
Merge
WT Sf
ΔmxiE Sf
-IFNγ
+IFNγ
10 µm
B
A549 cells
***
***
%Sf M1-Ub+
50
40
30
20
10
0
Sf:
WT
ΔmxiE
-IFNγ
+IFNγ
C
HT29 cells
****
****
%Sf M1-Ub+
25
20
15
10
5
0
Sf:
WT
ΔmxiE
-IFNγ
+IFNγ

Fig. 1

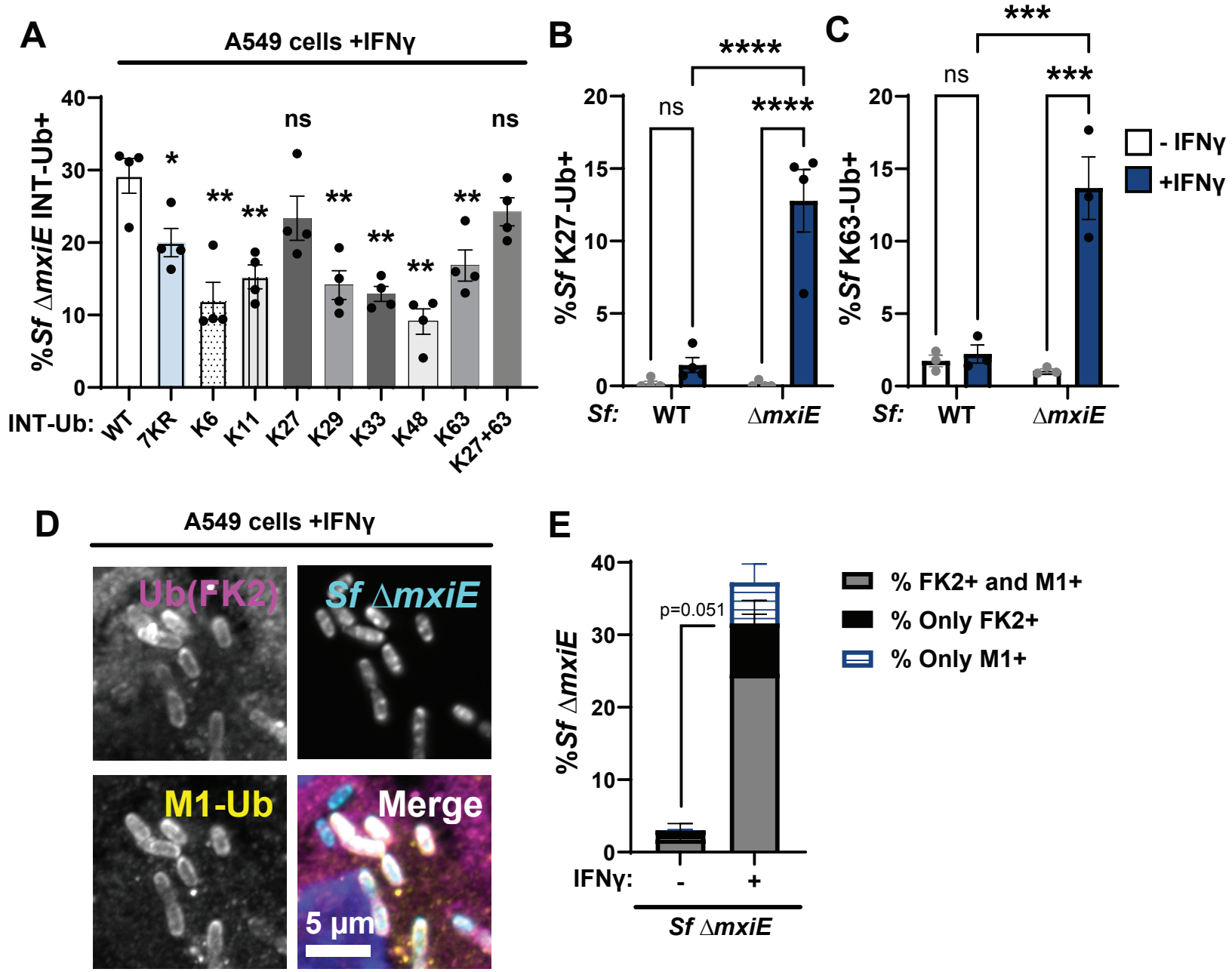
A
A549 cells +IFNγ
%Sf ΔmxiE INT-Ub+
INT-Ub:
WT
7KR
K6
K11
K27
K29
K33
K48
K63
K27+63
ns
B
%Sf K27-Ub+
Sf:
WT
ΔmxiE
C
%Sf K63-Ub+
- IFNγ
+IFNγ
D
A549 cells +IFNγ
Ub(FK2)
Sf ΔmxiE
M1-Ub
Merge
5 µm
E
%Sf ΔmxiE
p=0.051
% FK2+ and M1+
% Only FK2+
% Only M1+
IFNγ:
Sf ΔmxiE

Fig. 2

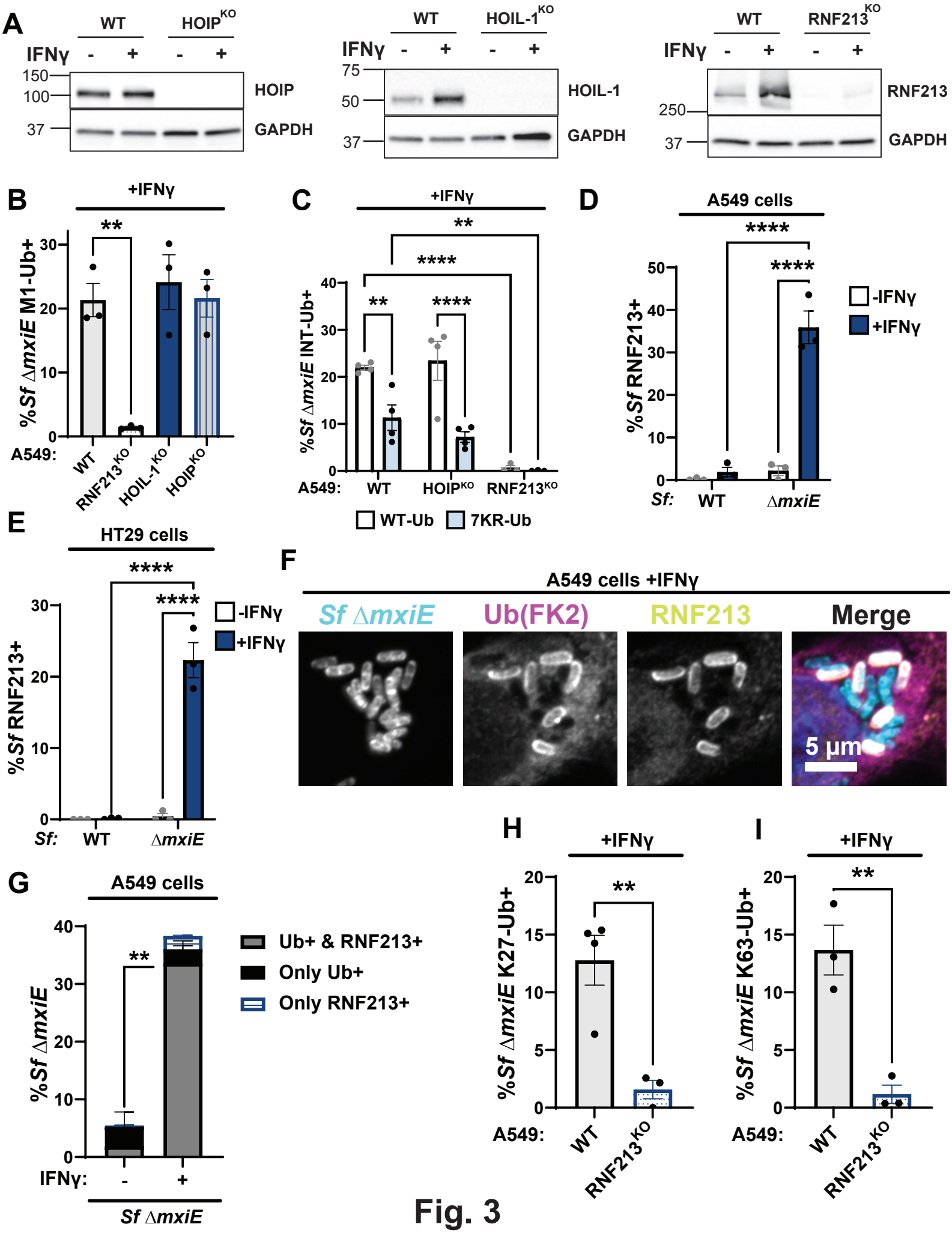
A
WT
HOIP^KO
IFNγ - + - +
150
100
37
HOIP
GAPDH
WT
HOIL-1^KO
IFNγ - + - +
75
50
37
HOIL-1
GAPDH
WT
RNF213^KO
IFNγ - + - +
250
37
RNF213
GAPDH
B
+IFNγ
**
%Sf ΔmxiE M1-Ub+
30
20
10
0
A549:
WT
RNF213^KO
HOIL-1^KO
HOIP^KO
C
+IFNγ
**
****
**
****
%Sf ΔmxiE INT-Ub+
40
30
20
10
0
A549:
WT
HOIP^KO
RNF213^KO
WT-Ub
7KR-Ub
D
A549 cells
****
****
%Sf RNF213+
50
40
30
20
10
0
-IFNγ
+IFNγ
Sf:
WT
ΔmxiE
E
HT29 cells
****
****
%Sf RNF213+
30
20
10
0
-IFNγ
+IFNγ
Sf:
WT
ΔmxiE
F
A549 cells +IFNγ
Sf ΔmxiE
Ub(FK2)
RNF213
Merge
5 µm
G
A549 cells
**
%Sf ΔmxiE
40
30
20
10
0
Ub+ & RNF213+
Only Ub+
Only RNF213+
IFNγ: - +
Sf ΔmxiE
H
+IFNγ
**
%Sf ΔmxiE K27-Ub+
20
15
10
5
0
A549:
WT
RNF213^KO
I
+IFNγ
**
%Sf ΔmxiE K63-Ub+
20
15
10
5
0
A549:
WT
RNF213^KO

Fig. 3

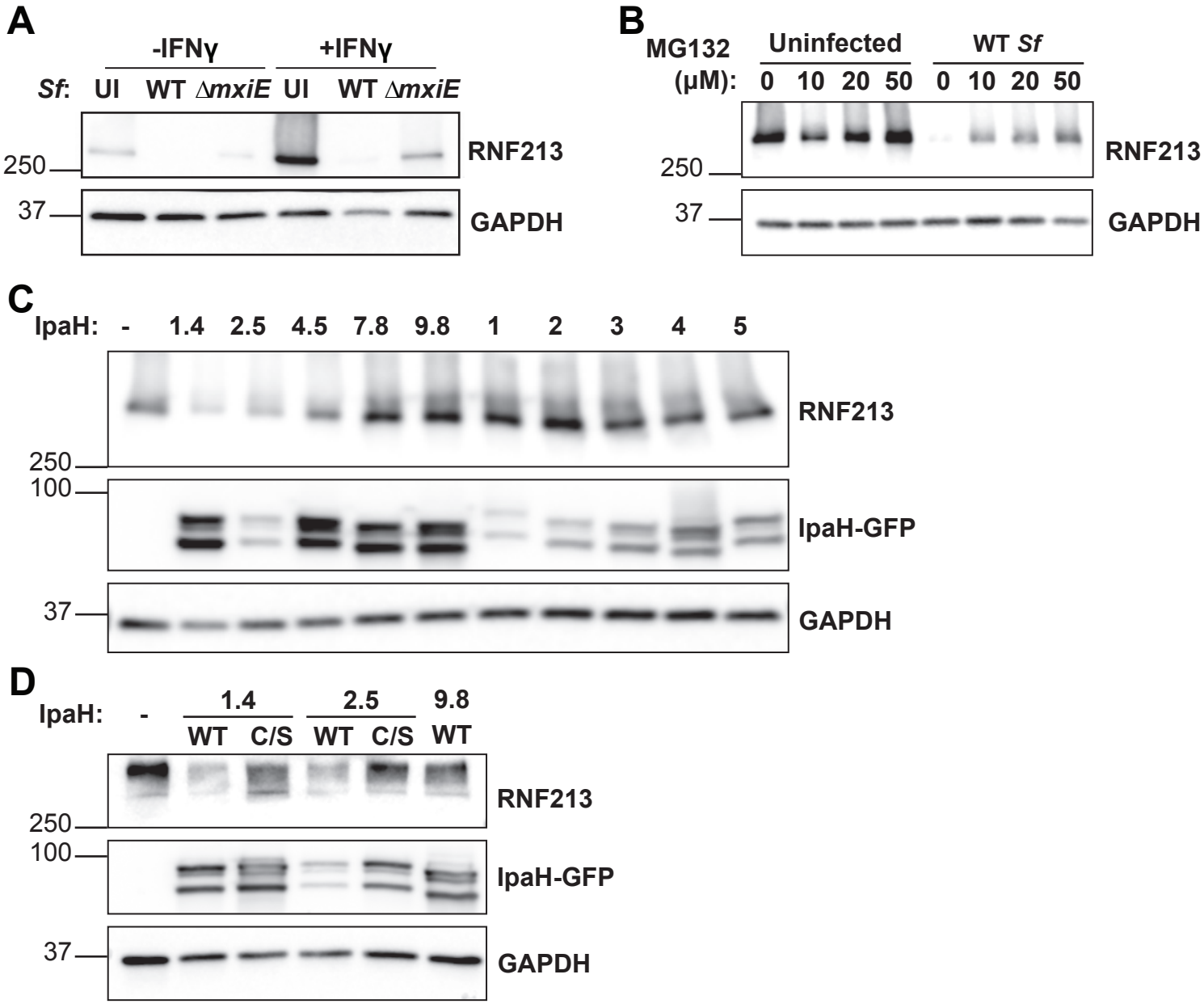
A
-IFNγ
+IFNγ
Sf: UI WT ΔmxiE UI WT ΔmxiE
250
37
RNF213
GAPDH
B
MG132 (μM):
Uninfected
WT Sf
0 10 20 50 0 10 20 50
250
37
RNF213
GAPDH
C
IpaH: - 1.4 2.5 4.5 7.8 9.8 1 2 3 4 5
250
100
37
RNF213
IpaH-GFP
GAPDH
D
IpaH: -
1.4
2.5
9.8
WT C/S WT C/S WT
250
100
37
RNF213
IpaH-GFP
GAPDH

Fig. 4

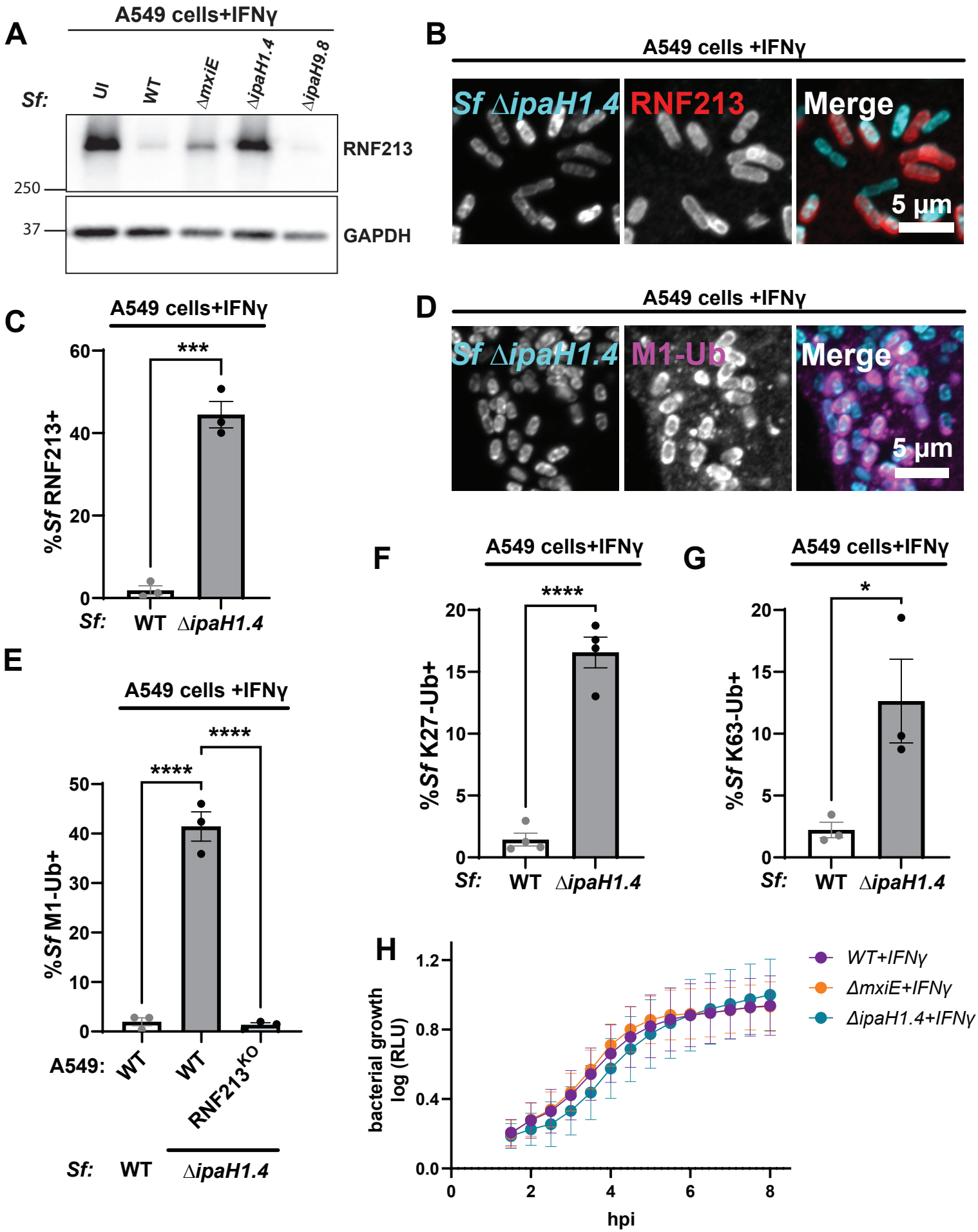
A
A549 cells+IFNγ
Sf:
UI
WT
ΔmxiE
ΔipaH1.4
ΔipaH9.8
RNF213
250
37
GAPDH
B
A549 cells +IFNγ
Sf ΔipaH1.4
RNF213
Merge
5 µm
C
A549 cells+IFNγ
***
%Sf RNF213+
60
40
20
0
Sf:
WT
ΔipaH1.4
D
A549 cells +IFNγ
Sf ΔipaH1.4
M1-Ub
Merge
5 µm
E
A549 cells +IFNγ
****
****
%Sf M1-Ub+
50
40
30
20
10
0
A549:
WT
WT
RNF213KO
Sf:
WT
ΔipaH1.4
F
A549 cells+IFNγ
****
%Sf K27-Ub+
20
15
10
5
0
Sf:
WT
ΔipaH1.4
G
A549 cells+IFNγ
*
%Sf K63-Ub+
20
15
10
5
0
Sf:
WT
ΔipaH1.4
H
bacterial growth
log (RLU)
1.2
0.8
0.4
0.0
0
2
4
6
8
hpi
WT+IFNγ
ΔmxiE+IFNγ
ΔipaH1.4+IFNγ

Fig. 5